

Momentum removal to obtain the position-dependent diffusion constant in constrained molecular dynamics simulation

Kazushi Fujimoto^{1*} | Tetsuro Nagai^{2*} | Tsuyoshi Yamaguchi^{3‡}

¹Department of Materials Chemistry, Graduate School of Engineering, Nagoya University, Nagoya, Aichi, 464-8603, Japan

²Department of Advanced Materials Science, Graduate School of Frontier Sciences, The University of Tokyo, Kashiwa, Chiba 277-8561, Japan

³Department of Materials Process Engineering, Graduate School of Engineering, Nagoya University, Nagoya, Aichi, 464-8603, Japan

Correspondence

Tsuyoshi Yamaguchi, Department of Materials Process Engineering, Graduate School of Engineering, Nagoya University, Nagoya, Aichi, 464-8603, Japan
Email:
yamaguchi.tsuyoshi@material.nagoya-u.ac.jp

Funding information

Japan Society for the Promotion of Science (JSPS), KAKENHI, Grant numbers: 19K03768 and 20K05631; Ministry of Education, Culture, Sports, Science and Technology (MEXT), Program for Promoting Researches on the Supercomputer Fugaku (No. JPMXP1020200308); The Nitto Foundation.

The position-dependent diffusion coefficient along with free energy profile are important parameters needed to study mass transport in heterogeneous systems such as biological and polymer membranes, and molecular dynamics (MD) calculation is a popular tool to obtain them. Among many methodologies, the Marrink–Berendsen (MB) method is often employed to calculate the position-dependent diffusion coefficient, in which the autocorrelation function of the force on a fixed molecule is related to the friction on the molecule. However, the diffusion coefficient is shown to be affected by the period of the removal of the center-of-mass velocity, τ_{v0} , which is necessary when performing MD calculations using the Ewald method for Coulombic interaction. We have clarified theoretically in this study how this operation affects the diffusion coefficient calculated by the MB method, and the theoretical predictions are proven by MD calculations. Therefore, we succeeded in providing guidance on how to select an appropriate τ_{v0} value in estimating the position-dependent diffusion coefficient by the MB

Abbreviations: COM, Center of mass; FACF, Force autocorrelation function; MB, Marrink–Berendsen; MD, Molecular Dynamics; WR, Woolf–Roux.

* Equally contributing authors.

method. This guideline is applicable also to the Woolf–Roux method.

KEYWORDS

Position-dependent diffusion coefficient, Marrink–Berendsen method, Woolf–Roux method, Molecular dynamics calculation

1 | INTRODUCTION

Mass transport phenomena in heterogeneous systems are important issues in various fields, and much research has been conducted in this area to date. For example, in the field of biological chemistry, understanding the permeation of drugs into viruses¹ and through membranes^{2–4} at the molecular level plays an important role in appropriate rational drug design. In the field of materials sciences such as in the separation of molecules using reverse osmosis membranes^{5,6} and the study of the transport process of protons, oxygen, and hydrogen in a polymer electrolyte membrane^{7–9}, it is important to understand the relationship between the mechanism molecular transport and the microscopic details of the materials.

The position-dependent diffusion coefficient, along with the free energy profile, is an important physical quantity utilized in studies of the mass transport phenomena of heterogeneous systems using molecular dynamics (MD) calculations. Because of its importance, many methods^{10–19} have been proposed to obtain the position-dependent diffusion coefficient. Two of us and other coworkers have also previously proposed a method for obtaining the position-dependent diffusion coefficient with high accuracy in any heterogeneous system²⁰. Among the methods proposed so far, the Marrink–Berendsen (MB) method is one of the best-known methods used to calculate the position-dependent diffusion coefficient^{21–26}.

Despite systematic underestimation^{27,20}, the method is widely used these days because the position-dependent diffusion coefficient can be calculated easily by the MB method with existing MD calculation packages. In the MB method, the center of mass (COM) of the molecule is constrained to a certain position, and the diffusion coefficient can be obtained by the force autocorrelation function (FACF) of the COM of the molecule.

In this paper, we demonstrate the critical role of momentum removal in obtaining the position-dependent diffusion coefficient by methods involving position constraints, such as the MB method. In MD calculations that use the Ewald method^{28,29} for calculating the long-range Coulombic interaction, the momentum of the MD system is reduced to zero with a certain time interval, τ_{v0} , to prevent the MD system from diffusing. We demonstrate that this operation affects the diffusion coefficient calculated by the MB method when constraining the diffusing molecules to absolute coordinates. In this paper, we propose a theoretical equation comparing FACFs with and without the COM momentum removal. The theoretical equation was then examined to find the diffusion coefficient of methane in water. It was also found that τ_{v0} dependence varies with the size of the system in the MD calculation. The theory we propose in this paper plays an important role in obtaining the position-dependent diffusion coefficient in three-dimensional heterogeneous systems using the MB method. The WR method with spring restraint on absolute values is also discussed.

2 | THEORY

The change in FCF, $\langle \mathbf{F}(0) \cdot \mathbf{F}(t) \rangle$, with changing τ_{v0} is explained qualitatively in terms of the momentum conservation within the whole simulation cell. Suppose that a solute molecule of infinite dilution feels force from the surrounding solvent in the $+z$ direction at $t = 0$. The force between the solute and the solvent means the momentum exchange between them, and the momentum in the $-z$ direction is then transferred from the solute to the solvent. The momentum given by the solvent is further transported to the bulk solvent with time through solvent-solvent interactions. In the MD simulation cell of finite size, however, the momentum in the $-z$ direction cannot dissipate due to the momentum conservation, and the momentum is instead distributed uniformly over the whole simulation cell after sufficient time, which means the solvent flows in the $-z$ direction. The fixed solute in the solvent flow in the $-z$ direction then feels frictional force in the $-z$ direction, leading to a negative correlation between $\mathbf{F}(0)$ and $\mathbf{F}(t)$. A shift of the COM velocity of the solvent eliminates the negative correlation, and its operation frequency, $1/\tau_{v0}$, affects the strength of the negative correlation at longer time durations. The physics concepts outlined above are described quantitatively hereafter in this section using projection operator formalism.

The system under consideration is composed of a solute (X) and a finite number of solvent molecules (S), which are contained in a cell with periodic boundary conditions. The solute is fixed at a given spatial position and no other external force operates on the solvent. A shift of the COM velocity of the solvent is not performed.

The COM velocity of the solvent, \mathbf{v}_{CM} , is defined as follows:

$$\mathbf{v}_{CM} \equiv \frac{1}{M_S} \sum_{i \in S} m_i \mathbf{v}_i, \quad (1)$$

$$M_S \equiv \sum_{i \in S} m_i. \quad (2)$$

Here, the summations run over all the solvent molecules, and the mass and the velocity of the i -th solvent molecule are described as m_i and \mathbf{v}_i , respectively. The projection operator onto \mathbf{v}_{CM} is defined as \mathcal{P} , and the projection operator to the orthogonal space is given by $\mathcal{Q} \equiv 1 - \mathcal{P}$.

An identity below holds for the time propagation operator as³⁰

$$e^{j\mathcal{L}t} \mathcal{Q} = e^{j\mathcal{Q}\mathcal{L}Q t} + \int_0^t d\tau e^{j\mathcal{L}(t-\tau)} \mathcal{P} j \mathcal{L} e^{j\mathcal{Q}\mathcal{L}Q\tau}, \quad (3)$$

where \mathcal{L} stands for the Liouvillian operator. Equation (3) is then multiplied by the force on the solute, \mathbf{F}_X , from the left to yield

$$\begin{aligned} e^{j\mathcal{L}t} \mathbf{F}_X &= e^{j\mathcal{Q}\mathcal{L}Q t} \mathbf{F}_X - \frac{M_S}{3k_B T} \int_0^t d\tau \left[e^{j\mathcal{L}(t-\tau)} \mathbf{v}_{CM} \right] \\ &\quad \times \left\langle \{ j \mathcal{L} \mathbf{v}_{CM} \} \cdot \left\{ e^{j\mathcal{Q}\mathcal{L}Q\tau} \mathbf{F}_X \right\} \right\rangle. \end{aligned} \quad (4)$$

The Boltzmann constant and the absolute temperature are denoted here as k_B and T , respectively.

The momentum conservation of the whole system relates \mathbf{F}_X and \mathbf{v}_{CM} as

$$\mathbf{F}_X + M_S \{ j \mathcal{L} \mathbf{v}_{CM} \} = 0, \quad (5)$$

80 which is substituted into Eq. (4) to give

$$e^{i\mathcal{L}t}\mathbf{F}_X = e^{iQ\mathcal{L}Q}t\mathbf{F}_X + \frac{1}{3k_B T} \int_0^t d\tau \left[e^{i\mathcal{L}(t-\tau)}\mathbf{v}_{CM} \right] \times \left\langle \left\{ i\mathcal{L}\mathbf{F}_X \right\} \cdot \left\{ e^{iQ\mathcal{L}Q\tau}\mathbf{F}_X \right\} \right\rangle. \quad (6)$$

81 We change the notations here as follows:

$$\mathbf{F}_X(t) \equiv e^{i\mathcal{L}t}\mathbf{F}_X, \quad (7)$$

$$\mathbf{R}_X(t) \equiv e^{iQ\mathcal{L}Q}t\mathbf{F}_X, \quad (8)$$

$$\mathbf{v}_{CM}(t) \equiv e^{i\mathcal{L}t}\mathbf{v}_{CM}, \quad (9)$$

$$\gamma(t) \equiv \frac{1}{3k_B T} \langle \mathbf{R}_X(0) \cdot \mathbf{R}_X(t) \rangle. \quad (10)$$

82 Equation (6) is then rewritten with these notations as

$$\mathbf{F}_X(t) = \mathbf{R}_X(t) + \int_0^t d\tau \gamma(t-\tau)\mathbf{v}_{CM}(\tau). \quad (11)$$

83 In Eq. (11), the total force acting on the solute at time t , $\mathbf{F}_X(t)$, is divided into the sum of random force, $\mathbf{R}_X(t)$, and
84 the drag force by the flow of the solvent.

85 The statistical average of Eq. (11) after the multiplication of $\mathbf{F}_X(0) = \mathbf{R}_X(0)$ gives

$$\langle \mathbf{F}_X(0) \cdot \mathbf{F}_X(t) \rangle = \langle \mathbf{R}_X(0) \cdot \mathbf{R}_X(t) \rangle + \int_0^t d\tau \gamma(t-\tau) \times \langle \mathbf{F}_X(0) \cdot \mathbf{v}_{CM}(\tau) \rangle. \quad (12)$$

86 The time correlation function in the integral, $\langle \mathbf{F}_X(0) \cdot \mathbf{v}_{CM}(\tau) \rangle$, is further related to FACF as

$$\langle \mathbf{F}_X(0) \cdot \mathbf{F}_X(t) \rangle + M_S \frac{d}{dt} \langle \mathbf{F}_X(0) \cdot \mathbf{v}_{CM}(t) \rangle = 0 \quad (13)$$

87 by virtue of Eq. (5).

88 The MB method is used to evaluate approximately the time correlation function of the random force acting on a
89 freely moving solute as that of the total force on the spatially fixed one¹¹. The time correlation function of the random
90 force is then converted into the time-dependent friction coefficient through Eq. (10), and the position-dependent
91 diffusion coefficient can then be determined. According to Eq. (12), however, the time correlation function of the
92 total force, $\langle \mathbf{F}_X(0) \cdot \mathbf{F}_X(t) \rangle$, contains the correlation with the drag force, in addition to the time correlation function
93 of the random force, $\langle \mathbf{R}_X(0) \cdot \mathbf{R}_X(t) \rangle$. What we actually want to determine is the latter correlation function, and we
94 need to somehow eliminate the second term of Eq. (12).

95 The time development of the random force is governed by the projected Liouvillian, $Q\mathcal{L}Q$, instead of the normal
96 one, \mathcal{L} . Since the dynamics of the random force are determined by that of the positions and the momenta of the
97 solvent molecules, $\{\mathbf{r}_i, \mathbf{p}_i\}$, the effects of the replacement of the Liouvillian can be analyzed through their dynamics.

98 The time dependence of \mathbf{r}_i and \mathbf{p}_i through QLQ is explicitly written as follows:

$$iQLQ\mathbf{r}_i = \frac{1}{m_i}\mathbf{p}_i - \frac{1}{M_S}\sum_{j\in S}\mathbf{p}_j, \quad (14)$$

$$iQLQ\mathbf{p}_i = \mathbf{F}_i - \frac{m_i}{M_S}\sum_{j\in S}\mathbf{F}_j, \quad (15)$$

99 where \mathbf{F}_i stands for the force acting on the solvent molecule i . In Eqs. (14) and (15), the first terms of the right-hand
100 sides give the ordinary time dependence through \mathcal{L} , and the second terms mean the shift of the COM velocity. There-
101 fore, the dynamics given by the projected Liouvillian, QLQ , corresponds to the time propagation of MD simulation in
102 which the shift of the COM velocity is performed at every step. It is thus expected that a smaller τ_{v0} leads to a better
103 diffusion coefficient in the implementation of the MB method in MD simulation.

104 The long-time limiting behaviors of $\langle \mathbf{F}_X(0) \cdot \mathbf{F}_X(t) \rangle$ can be analyzed based on Eqs. (12) and (13). First, the integral
105 of Eq. (13) from $t = 0$ to ∞ gives

$$\int_0^\infty dt \langle \mathbf{F}_X(0) \cdot \mathbf{F}_X(t) \rangle = M_S [\langle \mathbf{F}_X(0) \cdot \mathbf{v}_{CM}(0) \rangle - \langle \mathbf{F}_X(0) \cdot \mathbf{v}_{CM}(\infty) \rangle]. \quad (16)$$

106 The first term of the right-hand side vanishes so long as \mathbf{F}_X does not depend on the velocity of the solvent explicitly.
107 The second term is also zero because the correlation is lost after the infinite time interval. Therefore, the integral of
108 $\langle \mathbf{F}_X(0) \cdot \mathbf{F}_X(t) \rangle$ on the left-hand side is equal to zero. It should be noted that the discussion above does not apply to
109 an infinite-size system where M_S diverges.

110 The time derivative of Eq. (12), combined with Eq. (13) yields

$$\begin{aligned} \frac{d}{dt} \langle \mathbf{F}_X(0) \cdot \mathbf{F}_X(t) \rangle &= \frac{d}{dt} \langle \mathbf{R}_X(0) \cdot \mathbf{R}_X(t) \rangle \\ &\quad - \frac{1}{M_S} \int_0^t d\tau \gamma(t-\tau) \langle \mathbf{F}_X(0) \cdot \mathbf{F}_X(\tau) \rangle. \end{aligned} \quad (17)$$

111 Provided that the relaxation of $\gamma(t)$ is relatively fast, Eq. (17) can be approximated in the time scale longer than the
112 relaxation time of $\gamma(t)$ as

$$\begin{aligned} &\frac{d}{dt} \langle \mathbf{F}_X(0) \cdot \mathbf{F}_X(t) \rangle \\ &\simeq -\frac{1}{M_S} \left[\int_0^\infty d\tau \gamma(\tau) \right] \langle \mathbf{F}_X(0) \cdot \mathbf{F}_X(t) \rangle. \end{aligned} \quad (18)$$

113 It means that $\langle \mathbf{F}_X(0) \cdot \mathbf{F}_X(t) \rangle$ decays exponentially as

$$\langle \mathbf{F}_X(0) \cdot \mathbf{F}_X(t) \rangle \propto e^{-\frac{t}{\tau_{FF}}}, \quad (19)$$

114 with the time constant given by

$$\tau_{FF} = \frac{M_S}{\int_0^\infty d\tau \gamma(\tau)}. \quad (20)$$

3 | METHOD

3.1 | Molecular dynamics calculation

The effect of the frequency of the shift of the COM velocity on the time correlation function was investigated by performing simulations with different τ_{v0} values. Here, τ_{v0} denotes the interval between the removals of the COM velocity during MD simulations. System-size dependence was also investigated by studying two methane solutions of different sizes. The smaller system was composed of a methane molecule and 1053 water molecules and was simulated with τ_{v0} set at 1 fs, 0.1 ps, 10 ps, and ∞ . As to the larger system consisting of a methane molecule and 8424 water molecules, τ_{v0} was set at 0.1 ps, 10 ps, and ∞ . Since the time step of the MD simulation was set at 1 fs as described below, the simulation with $\tau_{v0} = 1$ fs corresponds to a faithful realization of the dynamics as defined by Eqs. 14 and 15, whereby $\mathbf{R}_X(t)$ can be directly and accurately evaluated. Moreover, simulations with $\tau_{v0} = \infty$ correspond to the dynamics defined by the Liouvillian operator. These simulations enable the measurement of $\mathbf{F}_X(t)$. Hereafter, the FACF obtained by MD with τ_{v0} is denoted by $C_{FF}^{\text{sim}}(t; \tau_{v0}) \equiv \langle \mathbf{F}^{\text{sim}}(t; \tau_{v0}) \cdot \mathbf{F}^{\text{sim}}(0; \tau_{v0}) \rangle$ to explicitly express the dependence on τ_{v0} .

After routine equilibration, each of the production runs was performed in the NVT ensemble for 50 ns with a time step of 1 fs. The temperature was controlled by a Nosé–Hoover thermostat^{31,32} at 300 K with a time constant of 100 fs. The effect of the thermostat on the resultant diffusion constant has been shown to be negligible in these conditions²⁰ for various methods, thus allowing us to get the position-dependent diffusion constant. The total force acting on the COM of the methane molecule was sampled every 1 fs. The electrostatic potential was calculated by the particle mesh Ewald method with a short-range cutoff length of 1.2 nm. The van der Waals interaction was cut off at 1.2 nm and the cutoff correction applied. All simulations were performed using GROMACS 2019³³, which was modified to constrain the methane molecule. The water molecules were modeled by the SPC model³⁴ and the methane molecule was modeled by OPLS-UA³⁵.

3.2 | Analysis

We demonstrated numerically the satisfaction of Eq. 12 and thereby the theoretical framework described in the aforementioned section. To achieve this, we evaluated $\langle \mathbf{F}_X(0) \cdot \mathbf{F}_X(t) \rangle$ and $\langle \mathbf{R}_X(0) \cdot \mathbf{R}_X(t) \rangle$. Given these time correlation functions, the integrand on the right hand-side of Eq. 12 can be obtained via Eqs. 10 and 13. In particular, $\langle \mathbf{F}_X(0) \cdot \mathbf{v}_{CM}(\tau) \rangle$ was obtained by integrating $\langle \mathbf{F}_X(0) \cdot \mathbf{F}_X(t) \rangle$ from zero to τ (see Eq. 13). The time correlation function $\langle \mathbf{F}_X(0) \cdot \mathbf{F}_X(t) \rangle$ was evaluated as $\langle \mathbf{F}^{\text{sim}}(t; \infty) \cdot \mathbf{F}^{\text{sim}}(0; \infty) \rangle$ or the force autocorrelation function obtained from the trajectories with $\tau_{v0} = \infty$, as these trajectories are the realization of dynamics of the Liouvillian operator. As regards the smaller system, $\langle \mathbf{R}_X(0) \cdot \mathbf{R}_X(t) \rangle$ was calculated from the trajectory with $\tau_{v0} = 1$ fs, which is a faithful realization of the dynamics defined by Eqs. 14 and 15. In other words, $\langle \mathbf{R}_X(0) \cdot \mathbf{R}_X(t) \rangle$ was calculated by $\langle \mathbf{F}^{\text{sim}}(t; 1 \text{ fs}) \cdot \mathbf{F}^{\text{sim}}(0; 1 \text{ fs}) \rangle$. For the larger system, $\langle \mathbf{R}_X(0) \cdot \mathbf{R}_X(t) \rangle$ was substituted by the FACF obtained for $\tau_{v0} = 0.1$ ps, $\langle \mathbf{F}^{\text{sim}}(t; 0.1 \text{ ps}) \cdot \mathbf{F}^{\text{sim}}(0; 0.1 \text{ ps}) \rangle$, which was found to approximate well the dynamics defined by Eqs. 14 and 15, as described in the following section. In these calculations, the numerical integration was performed using the trapezoidal formula.

150 4 | RESULTS AND DISCUSSION

151 4.1 | Smaller system

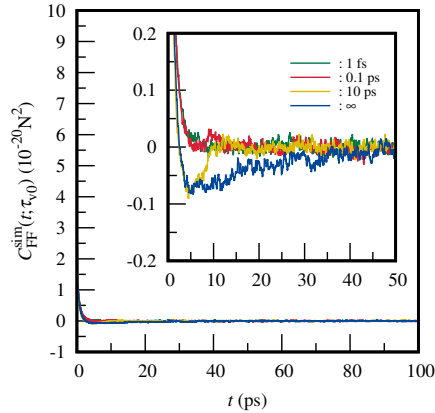


FIGURE 1 Time correlation function of the force on the methane molecule at $\tau_{v0} = 1$ fs (green), 0.1 ps (red), 10 ps (yellow), and ∞ (blue) in the smaller system. The inset shows a magnified view for $0 \leq t \leq 50$ ps.

152 Figure 1 shows time correlation functions of the force on the methane molecule at $\tau_{v0} = 1$ fs, 0.1 ps, 10 ps, and
 153 ∞ in the smaller system. This graph shows that the time correlation function for $\tau_{v0} \leq 0.1$ ps converged to zero
 154 immediately. On the other hand, a negative correlation appears for $\tau_{v0} \geq 10$ ps. Considering that the absence of the
 155 negative tail for the systems of $\tau_{v0} = 1$ fs and 0.1 ps can be ascribed to the fast decay of the tail, the larger τ_{v0} is,
 156 the more slowly the negative correlation relaxes. The negative correlation for $\tau_{v0} = 10$ ps disappears at approximately 10
 157 ps. This means that the effect of the momentum given by the solute to the solvent disappears due to the shift in the
 158 COM velocity at times longer than τ_{v0} . The MB method calculates the diffusion coefficient by

$$D = \frac{3(k_B T)^2}{\int_0^\infty \langle \Delta \mathbf{F}_X(0) \cdot \Delta \mathbf{F}_X(t) \rangle dt}. \quad (21)$$

159 Here, Δ is appended to $\mathbf{F}_X(t)$ to describe explicitly the deviation from the mean force, however, Δ can be omitted
 160 in homogeneous systems as considered in this work. Equation 21 indicates that the diffusion coefficient is inversely
 161 proportional to the integrated value of FACF. Therefore, the fact that the shape of the time correlation function in
 162 Fig. 1 differs depending on τ_{v0} means that the calculated diffusion coefficient also differs depending on τ_{v0} .

163 Figure 2 shows the running integrals of the time correlation functions of the force at $\tau_{v0} = 1$ fs, 0.1 ps, 10 ps,
 164 and ∞ in the smaller system. When the time correlation function of the force converges to zero, the integrated
 165 value converges to a certain value. By substituting this converged value into Eq. 21, the diffusion coefficient can be
 166 estimated, and Fig. 2 clearly shows that the converged values differ depending on τ_{v0} . As mentioned in Section 2, the
 167 integral converges to the correct value when the COM velocity of the system is removed at every step. Therefore,
 168 the converged integral value at $\tau_{v0} = 1$ fs is correct. For $\tau_{v0} \leq 0.1$ ps, the running integral converged to the same
 169 value as that at $\tau_{v0} = 1$ fs. This means that $\tau_{v0} = 0.1$ ps would be sufficiently small to give accurate results for the size

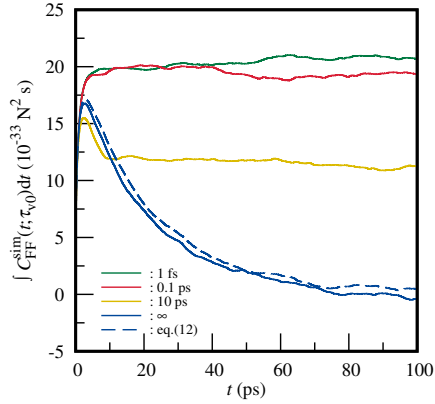


FIGURE 2 Running integrals of the time correlation function of the force on the methane molecule at $\tau_{v0} = 1$ fs (green), 0.1 ps (red), 10 ps (yellow), and ∞ (blue) in the smaller system. The curve calculated by the right-hand side of Eq. 12 is shown by the blue dashed line.

170 of the system in this MD calculation. As τ_{v0} increases, the converged value became smaller and smaller, and $\tau_{v0} = \infty$
 171 converges to 0, which is consistent with Eq. 16. The physical explanation is that the momentum given by the solute
 172 to the solvent is finally returned to the solute, because $\tau_{v0} = \infty$ means the absence of a momentum sink other than
 173 the solute itself. Moreover, comparing the functional form of the calculation result until it converges to zero with the
 174 result from the theoretical equation (Eq. 12), the curve at $\tau_{v0} = \infty$ is consistent with the curve obtained from the
 175 theoretical equation. Therefore, the numerical calculations support the validity of our theory. In other words, the
 176 theory elucidates that the diffusion coefficient from the MB method depends on the period (τ_{v0}) in which the COM
 177 velocity is removed during MD simulations. The theory thus captures the physical mechanism by which the choice of
 178 τ_{v0} affects the FACFs through the modification of the correlation functions.

179 4.2 | Larger system

180 Time correlation functions of the force on the methane molecule and their running integrals are shown in Figs. 3 and
 181 4, respectively, at $\tau_{v0} = 0.1$ ps, 10 ps, and ∞ in the larger system. Figure 3 shows that the negative correlation is
 182 weaker than that of the smaller system. As the MD system size increases, the momentum of the system is distributed
 183 over a larger space, and the COM velocity of the solvent generated by the momentum given by the solute becomes
 184 smaller. Therefore, the dependence on τ_{v0} becomes smaller as the system size of the MD calculations increases. For
 185 $\tau_{v0} = \infty$, the negative correlation is weaker than that in the smaller system, but its relaxation becomes slower, as
 186 shown in Figure 4. Eq. 16 predicts theoretically that the running integral at $\tau_{v0} = \infty$ should converge to zero for any
 187 finite systems, but unlike the smaller system, here the convergence was not complete even at 100 ps. The reason
 188 for this slow relaxation is that the larger the system, the longer it takes for the momentum to return. The agreement
 189 between the MD simulation and the theoretical prediction of Eq. 12 is excellent, also in the larger system, Fig. 4,
 190 which further supports our theoretical discussion. Figure 4 shows that, for the larger system, the result with $\tau_{v0} = 10$
 191 ps was close to the correct value ($\tau_{v0} = 0.1$ ps). Therefore, the larger the system size, the larger τ_{v0} can be set.

192 According to Eq. 20, the τ_{FF} of the small and large systems were 19.1 and 174.7 ps, respectively. Eq. 19 is plotted

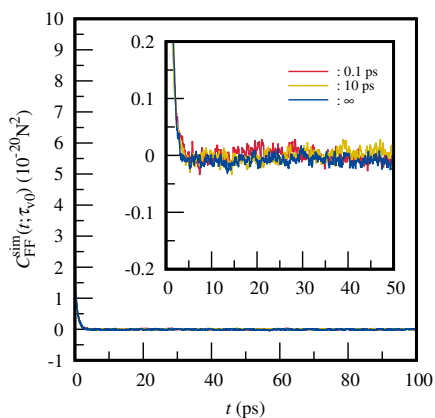


FIGURE 3 Time correlation function of the force on the methane molecule at $\tau_{v0} = 0.1$ ps (red), 10 ps (yellow), and ∞ (blue) in the large system. The inset shows a magnified view for $0 \leq t \leq 50$ ps.

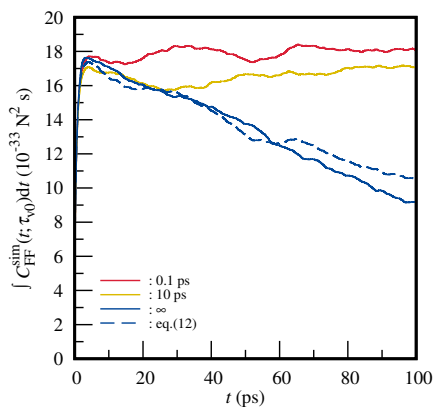


FIGURE 4 Integrating the time correlation function of the force on the methane molecule at $\tau_{v0} = 0.1$ ps (red), 10 ps (yellow), and ∞ (blue) in the large system. The curve calculated by Eq. 12 is shown by the blue dotted line.

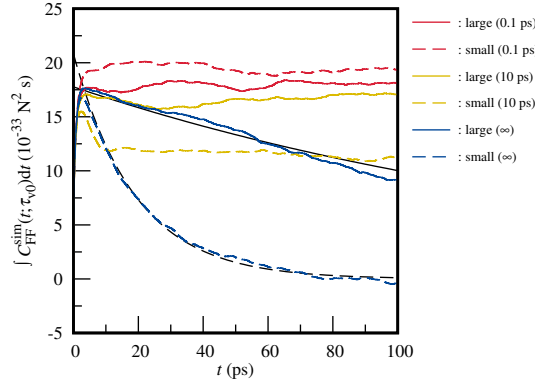


FIGURE 5 Integrating the time correlation function of the force on the methane molecule at $\tau_{v0} = 0.1$ ps (red), 10 ps (yellow), and ∞ (blue) in the large (solid line) and small (dashed line) systems. Eq. (19) of the large and small systems is shown by black solid and dashed lines.

193 using these τ_{FF} and regarding the amplitude as an adjustable parameter. In addition, the running integrals of the time
 194 correlation functions of the force on COM of the methane molecule in the larger and smaller systems are shown again
 195 in Fig. 5 to make their difference clearly visible. It can be seen that Eq. 18 reproduces the decay well at $\tau_{v0} = \infty$ for
 196 both the smaller and larger systems. τ_{FF} is a reference quantity for determining τ_{v0} , and the larger the τ_{FF} , the larger
 197 the value of τ_{v0} can be set. The larger the size of the system, the larger the value of τ_{FF} , which shows that τ_{v0} can be
 198 larger for larger systems. We mentioned in Section 4.2 that $\tau_{v0} = 0.1$ ps, which is one two-hundredths of τ_{FF} , is small
 199 enough to calculate D in the smaller system with sufficient accuracy. It is thus sufficient to set τ_{v0} to 1/200th of τ_{FF}
 200 even for a small system with fast decay. In the larger system, the result of $\tau_{v0} = 10$ ps, which is about 1/20th of τ_{FF}
 201 of the system, is close to that of $\tau_{v0} = 0.1$ ps. Therefore, it is safe to set τ_{v0} to at most 1/200th of τ_{FF} for any system
 202 larger than the smaller system.

203 For $\tau_{v0} \geq 10$ ps, the integral was larger for the larger system than that for the smaller one, indicating that the
 204 larger the size of the system, the longer the time part was affected, as discussed previously. However, at $\tau_{v0} = 0.1$
 205 ps, the integral of the smaller system was larger than that of the larger system. This is not an effect of the shift of
 206 the COM velocity, but that of the hydrodynamic interaction between the solutes in adjacent cells in the periodic
 207 boundary system. Due to the effects of hydrodynamic interaction, the diffusion coefficient, D_{MD} , calculated from the
 208 MD calculation of the finite system with periodic boundary conditions, is shifted from the true diffusion coefficient
 209 D_0 of the system of infinite size as shown in the following equation³⁶:

$$D_{MD} = D_0 - \frac{2.83729k_B T}{6\pi\mu L} \quad (22)$$

210 where μ and L are the viscosity coefficient and the length of the MD cell, respectively. This equation states that
 211 the smaller the cell size, the smaller D_{MD} becomes. Since the integral value of the time correlation function of the
 212 force is the reciprocal of D_{MD} (see Eq. 21), it becomes larger for smaller systems. Using the experimental viscosity
 213 coefficient of water at 25 °C ($\mu = 0.0009$ Pa·s) and Eq. 22, the difference in the integrated values of the time correlation
 214 functions of the force between the larger and the smaller systems was calculated to be $1 \times 10^{-10} \text{ m}^2 \cdot \text{s}^{-1}$. On the
 215 other hand, the difference found from our calculation, shown in Fig.5, is $2 \times 10^{-10} \text{ m}^2 \cdot \text{s}^{-1}$. So, the estimates from

216 the theoretical equations of fluid mechanics and our calculation are in good agreement, considering the error guessed
217 from the fluctuation of the running integral.

218 4.3 | Relevance to NVE ensemble and other thermostats

219 The formalized theory perfectly fits with the NVE ensemble, and thus the COM velocity shift is needed to eliminate the
220 unwanted negative correlation between $\mathbf{F}(0)$ and $\mathbf{F}(t)$. However, the shift decreases the total energy when applied
221 to the NVE simulations and therefore the simulations cannot reach thermal equilibrium. Furthermore, this decrease
222 can cause a drop in the temperature and thus the diffusion constant can be underestimated. It should be carefully
223 confirmed that the drift of the total energy or temperature is so marginal that the potential systematic error is satis-
224 factorily small in application to NVE simulations. Given this potential artifact that is intrinsic to the NVE simulations,
225 the coupling of a thermostat should be a practical choice, especially for long simulations, although disturbance from
226 a thermostat to the original dynamics needs to be carefully considered. We have performed NVT simulations using a
227 Nosé–Hoover thermostat in this work, and demonstrated that the discussion based on the NVE ensemble holds. We
228 next discuss the applicability of the COM velocity shift to thermostats other than the Nosé–Hoover thermostat. Other
229 widely used thermostats include the Gaussian constraint^{37–40}, velocity rescaling⁴¹, and a Langevin thermostat²⁹.

230 A COM velocity shift is necessary for the thermostats that retain linear momentum conservation, such as the
231 Gaussian constraint^{37–40} and velocity rescaling⁴¹, because the unwanted negative correlation between $\mathbf{F}(0)$ and
232 $\mathbf{F}(t)$ arises ultimately from the momentum conservation (Eq. 5) in a finite system as described above. Furthermore,
233 we have demonstrated numerically the necessity of the COM velocity shift for the Nosé–Hoover thermostat, which
234 also retains the momentum conservation. When it comes to thermostats that break the momentum conservation,
235 including the Langevin thermostat, we need to give more subtle consideration as follows.

236 When applying the Langevin thermostat, the coupling time constant τ_{LT} ($\tau_{LT} \equiv 1/\gamma$, where γ is the damping
237 coefficient of the thermostat) needs to be considered, as the thermostat works also as the momentum sink with this
238 time constant τ_{LT} . If the coupling is sufficiently strong, i.e., $\tau_{LT} \ll \tau_{FF}$, the diminishing behavior of the running integral
239 of $\langle \mathbf{F}_X(t) \cdot \mathbf{F}_X(0) \rangle$ should not be observed, because the COM momentum drops quickly. Nevertheless, because such
240 a strong coupling might disturb the short-term dynamics as well, the potential artifact in the diffusion constant should
241 be considered carefully. If the coupling is weak such that $\tau_{LT} \gg \tau_{FF}$, the running integral of $\langle \mathbf{F}_X(t) \cdot \mathbf{F}_X(0) \rangle$ should
242 diminish, as the momentum drops too slowly. In this case, the COM velocity shift should be performed frequently
243 enough such that $\tau_{v0} \ll \tau_{FF}$, even with this thermostat.

244 4.4 | Discussion on how to constrain the solute

245 4.4.1 | Harmonic constraint

246 The method proposed by Woolf and Roux (WR method) is another popular method for evaluating the position-
247 dependent diffusion coefficient¹². In the WR method, the solute is constrained around a position of interest by a
248 harmonic potential, and the spring constant of the potential, k , is an adjustable parameter. We hereafter discuss how
249 the COM velocity shift of the solvent affects the diffusion coefficient when the solute is constrained to absolute co-
250 ordinates in the WR method. For simplicity, we consider a homogeneous system where no potential of mean force is
251 induced on the solute by the solvent. When the system size is infinite, the dynamics of the solute in the WR method

252 is described by the generalized Langevin equation as

$$\dot{\mathbf{r}}_X(t) = \mathbf{v}_X(t), \quad (23)$$

$$m_X \dot{\mathbf{v}}_X(t) = \mathbf{F}_X(t), \quad (24)$$

$$\mathbf{F}_X(t) = \mathbf{R}_X(t) - \int_0^t d\tau \gamma(t-\tau) \mathbf{v}_X(\tau) - k \mathbf{r}_X(t). \quad (25)$$

253 Here, the mass, position, and velocity of the solute are denoted as m_X , $\mathbf{r}_X(t)$, and $\mathbf{v}_X(t)$, respectively, and the solute
254 is assumed to be constrained to the origin. The equations above are solved to yield the time correlation function of
255 the position as

$$\int_0^\infty dt \langle \mathbf{r}_X(0) \cdot \mathbf{r}_X(t) \rangle = \frac{\tilde{\gamma}_0}{k} \langle |\mathbf{r}_X(0)|^2 \rangle, \quad (26)$$

$$\tilde{\gamma}_0 \equiv \int_0^\infty dt \gamma(t). \quad (27)$$

256 Substituting the relationship between the fluctuation of the position and k as

$$\langle |\mathbf{r}_X(0)|^2 \rangle = \frac{3k_B T}{k}, \quad (28)$$

257 the diffusion coefficient is determined by the equation as follows:

$$D = \frac{k_B T}{\tilde{\gamma}_0} = \frac{\langle |\mathbf{r}_X(0)|^2 \rangle^2}{3 \int_0^\infty dt \langle \mathbf{r}_X(0) \cdot \mathbf{r}_X(t) \rangle}. \quad (29)$$

258 Next we consider the finite-size system, to which the shift of the COM velocity of the solvent is applied with a
259 time interval of τ_{v0} . Then, Eqs. 23 and 24 are intact, and Eq. 25 is modified as

$$\mathbf{F}_X(t) = \mathbf{R}_X(t) - \int_0^t d\tau \gamma(t-\tau) (\mathbf{v}_X(\tau) - \mathbf{v}_{CM}(\tau)) - k \mathbf{r}_X(t), \quad (30)$$

$$M_S \dot{\mathbf{v}}_{CM}(t) = -[\mathbf{F}_X(t) + k \mathbf{r}_X(t)] - \gamma_s M_S \mathbf{v}_{CM}(t). \quad (31)$$

260 Here, the shift of the COM velocity is approximated as the damping with a time constant of $\tau_{v0} = 1/\gamma_s$. The time
261 correlation function of the position is then obtained from Eqs. 23, 24, 30, and 31 as

$$\langle \mathbf{r}_X(0) \cdot \mathbf{r}_X(t) \rangle = \frac{\tilde{\gamma}_0}{k \left(1 + \frac{\tilde{\gamma}_0}{M_S \gamma_s}\right)} \langle |\mathbf{r}_X(0)|^2 \rangle. \quad (32)$$

262 Comparing Eqs. 26 and 32, it is shown that the WR method gives the correct value of the diffusion coefficient under
263 the condition as

$$\tau_{v0} = \frac{1}{\gamma_s} \ll \frac{M_S}{\tilde{\gamma}_0}, \quad (33)$$

264 which is the same condition as the MB method.

265 It is rather surprising that the condition Eq. 33 does not contain k . One may consider that τ_{v0} can be smaller
266 with decreasing k , because the diffusion coefficient from the WR method reduces to that from the mean square

267 displacement of the unconstrained solute, for which the shift of the COM velocity is unnecessary. However, Eq. 33
268 means that the removal of the COM velocity is indispensable in the WR method, irrespective of the strength of the
269 constraining potential. The result above indicates that the COM velocity of the solvent should be removed with
270 sufficient frequency when the solute is constrained to absolute coordinates, irrespective of how the constraint is
271 performed.

272 4.4.2 | Constraint by relative coordinates

273 Instead of constraining to absolute coordinates, it is also common to constrain the relative coordinates of two sub-
274 stances in order to calculate the position-dependent diffusion coefficients in heterogeneous systems. For example,
275 membrane permeation⁴² or substrate adsorption⁴³ of small molecules, and the transport across a transmembrane
276 channel of ions⁴⁴ are all discussed in terms of potential mean force (PMF) and the position-dependent relative diffu-
277 sion coefficient between two substances such as a membrane and a molecule.

278 In this case, external forces do not work, and only internal forces do. Therefore, the two terms on the left side
279 of Eq. 6 are both zero. Momentum does not flow toward the solvent, and the error discussed in this paper does not
280 occur. Therefore, τ_{v0} can be determined solely by considering its original purpose to compensate the numerical errors
281 in the Ewald calculation.

282 5 | CONCLUSION

283 It was shown theoretically that the position-dependent diffusion coefficient obtained using the MB method depends
284 on τ_{v0} . For systems as small as 1000 molecules, the FACS integrals converge well at $\tau_{v0} \leq 0.1$ ps, indicating that the
285 diffusion coefficient can be obtained with good accuracy. However, at $\tau_{v0} \geq 10$ ps, the integral converges to a value
286 different from the correct one. The larger was τ_{v0} , the smaller the converged value of the FACS integral became. The
287 converged value was zero at $\tau_{v0} = \infty$, which has good consistency with the theoretical prediction, thereby supporting
288 the validity of our theory.

289 For a system as large as 8000 molecules, the converged value of the FACS integral was close to the correct one
290 even when τ_{v0} was as large as 10 ps. In addition, the convergence of the integrated value became slower at $\tau_{v0} = \infty$.
291 This result is also consistent with our theoretical prediction, and shows that our theory is applicable, irrespective of
292 the system size. These calculations demonstrate the necessity of choosing τ_{v0} according to the size of the system
293 when calculating the position-dependent diffusion coefficient by the MB method using MD calculation with the Ewald
294 method. From the point of view of the speed of MD calculation, removing the COM velocity of the system requires
295 full communication between nodes of parallel computers, which slows down the calculation speed. Therefore, τ_{v0} is
296 preferred to be as large as possible, but 0.1 ps is probably sufficient for ordinary systems.

297 Acknowledgments

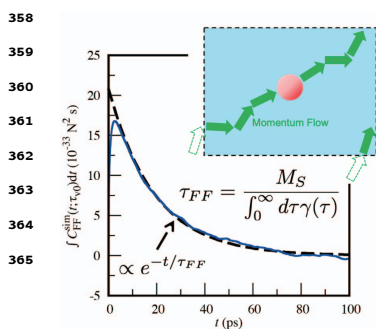
298 TY was supported by a Grant-in-aid (KAKENHI) from Japan Society for the Promotion of Science (JSPS) (Grant No.
299 19K03768). KF was supported by KAKENHI from JSPS (Grant No. 20K05631) and MEXT as "Program for Promoting
300 Researches on the Supercomputer Fugaku" (Environmentally benign functional chemicals: No. JPMXP1020200308).
301 This work is also partially supported by the Nitto Foundation. We also thank the Research Center for Computational
302 Science, Okazaki, Japan, for the use of its supercomputers.

303 **references**

- 304 [1] Fujimoto, K., Fukai, M., Urano, R., Shinoda, W., Ishikawa, T., Omagari, K., Tanaka, Y., Nakagawa, A. and Okazaki, S., *Pure*
305 *Appl. Chem.*, 2020, **92**(10), 1585–1594.
- 306 [2] Shinoda, W., *Biochim. Biophys. Acta, Biomembr.*, 2016, **1858**(10), 2254–2265.
- 307 [3] Awoonor-Williams, E. and Rowley, C. N., *Biochim. Biophys. Acta, Biomembr.*, 2016, **1858**(7), 1672–1687.
- 308 [4] Venable, R. M., Krämer, A. and Pastor, R. W., *Chem. Rev.*, 2019, **119**(9), 5954–5997.
- 309 [5] Shen, M., Keten, S. and Lueptow, R. M., *J. Membr. Sci.*, 2016, **506**, 95–108.
- 310 [6] Surblys, D., Yamada, T., Thomsen, B., Kawakami, T., Shigemoto, I., Okabe, J., Ogawa, T., Kimura, M., Sugita, Y. and Yagi,
311 K., *J. Membr. Sci.*, 2020, **596**, 117705.
- 312 [7] Kawakami, T. and Shigemoto, I., *Polymer*, 2014, **55**(24), 6309–6319.
- 313 [8] Kawakami, T., Shigemoto, I. and Matubayasi, N., *J. Chem. Phys.*, 2018, **148**(21), 214903.
- 314 [9] Takeuchi, K., Kuo, A.-T., Hirai, T., Miyajima, T., Urata, S., Terazono, S., Okazaki, S. and Shinoda, W., *J. Phys. Chem. C*, 2019,
315 **123**(33), 20628–20638.
- 316 [10] Straub, J. E., Borkovec, M. and Berne, B. J., *J. Phys. Chem.*, 1987, **91**, 4995–4998.
- 317 [11] Marrink, S.-J. and Berensen, H. J. C., *J. Phys. Chem.*, 1994, **98**, 4155–4168.
- 318 [12] Woolf, T. B. and Roux, B., *J. Am. Chem. Soc.*, 1994, **116**(13), 5916–5926.
- 319 [13] Hummer, G., *New J. Phys.*, 2005, **7**(1), 34.
- 320 [14] Sicard, F., Koskin, V., Annibale, A. and Rosta, E., *J. Chem. Theory Comput.*, 2021, **17**(4), 2022–2033.
- 321 [15] Yang, S., Onuchic, J. N., García, A. E. and Levine, H., *J. Mol. Biol.*, 2007, **372**(3), 756–763.
- 322 [16] Hinczewski, M., Hansen, Y. v., Dzubiella, J. and Netz, R. R., *J. Chem. Phys.*, 2010, **132**(24), 245103.
- 323 [17] Schulz, R., Yamamoto, K., Klossek, A., Flesch, R., Hönzke, S., Rancan, F., Vogt, A., Blume-Peytavi, U., Hedtrich, S., Schäfer-
324 Korting, M., Rühl, E. and Netz, R. R., *Proc. Natl. Acad. Sci. U. S. A.*, 2017, **114**(14), 3631–3636.
- 325 [18] Comer, J., Chipot, C. and González-Nilo, F. D., *J. Chem. Theory Comput.*, 2013, **9**(2), 876–882.
- 326 [19] Türkcan, S., Alexandrou, A. and Masson, J.-B., *Biophys. J.*, 2012, **102**(10), 2288–2298.
- 327 [20] Nagai, T., Tsurumaki, S., Urano, R., Fujimoto, K., Shinoda, W. and Okazaki, S., *J. Chem. Theory Comput.*, 2020, **16**, 7239–
328 7254.
- 329 [21] Liu, H.-S., Chen, K.-Y., Fang, C.-E. and Chiu, C.-c., *Electrochim. Acta*, 2021, **375**, 137915.
- 330 [22] Manrique, R., Wu, W. and Chang, J.-S., *J. Appl. Phycol.*, 2020, **32**(1), 291–297.
- 331 [23] Rivel, T., Ramseyer, C. and Yesylevskyy, S., *Sci. Rep.*, 2019, **9**(1), 5627.
- 332 [24] Yesylevskyy, S., Rivel, T. and Ramseyer, C., *Sci. Rep.*, 2019, **9**(1), 17214.
- 333 [25] Yang, H., Zhou, M., Li, H., Liu, L., Zhou, Y. and Long, X., *RSC Adv.*, 2019, **9**(67), 39046–39054.
- 334 [26] Manrique, R., Chang, J. and Wu, W., *IOP Conf. Ser.: Earth Environ. Sci.*, 2019, **268**(1), 012062.

- 335 [27] Daldrop, J. O., Kowalik, B. G. and Netz, R. R., *Phys. Rev. X*, 2017, **7**(4), 041065.
- 336 [28] Ewald, P. P., *Ann. Phys. (Berlin, Ger.)*, 1921, **369**(3), 253–287.
- 337 [29] Allen, M. P.; Tildesley, D. J., In *Computer Simulation of Liquids*; OXFORD University Press, Great Clarendon Street,
338 Oxford, OX2 6DP, United Kingdom, second ed., 2017.
- 339 [30] Balucani, U.; Zoppi, M., In *Dynamics of the Liquid State*; Oxford University Press, Great Clarendon Street, Oxford, OX2
340 6DP, United Kingdom, 1994.
- 341 [31] Nosé, S., *Mol. Phys.*, 1984, **52**, 255–268.
- 342 [32] Hoover, W., *Phys. Rev. A*, 1985, **31**, 1695–1697.
- 343 [33] Abraham, M. J., Murtola, T., Schulz, R., Páll, S., Smith, J. C., Hess, B. and Lindah, E., *SoftwareX*, 2015, **1-2**, 19–25.
- 344 [34] Berendsen, H. J. C., Postma, J. P. M., van Gunsteren, W. F. and Hermans, J. In *Intermolecular Forces*, Pullman, B., Ed.;
345 Springer, Dordrecht, Holland, 1981; pages 331–342.
- 346 [35] Jorgensen, W. L., Madura, J. D. and Swenson, C. J., *J. Am. Chem. Soc.*, 1984, **106**, 6638–6646.
- 347 [36] Yeh, I.-C. and Hummer, G., *J. Phys. Chem. B*, 2004, **108**(40), 15873–15879.
- 348 [37] Hoover, W. G., Ladd, A. J. and Moran, B., *Phys. Rev. Lett.*, 1982, **48**, 1818–1820.
- 349 [38] Evans, D. J., Hoover, W. G., Failor, B. H., Moran, B. and Ladd, A. J. C., *Phys. Rev. A*, 1983, **28**, 1016–1021.
- 350 [39] Zhang, F., *J. Chem. Phys.*, 1997, **106**, 6102–6106.
- 351 [40] Minary, P., Martyna, G. J. and Tuckerman, M. E., *J. Chem. Phys.*, 2003, **118**, 2510.
- 352 [41] Bussi, G., Donadio, D. and Parrinello, M., *J. Chem. Phys.*, 2007, **126**, 014101.
- 353 [42] Lee, C. T., Comer, J., Herndon, C., Leung, N., Pavlova, A., Swift, R. V., Tung, C., Rowley, C. N., Amaro, R. E., Chipot, C.,
354 Wang, Y. and Gumbart, J. C., *J. Chem. Inf. Model.*, 2016, **56**(4), 721–733.
- 355 [43] Ren, K., Wang, Y.-P. and Liu, S., *Phys. Chem. Chem. Phys.*, 2020, **23**(2), 1092–1102.
- 356 [44] Ngo, V., Li, H., MacKerell, A. D., Allen, T. W., Roux, B. and Noskov, S., *J. Chem. Theory Comput.*, 2021, **17**(3), 1726–1741.

357 GRAPHICAL ABSTRACT



The position-dependent diffusion coefficient is beneficial for studying mass transport with molecular dynamics calculations. In the Marrink–Berendsen method, this coefficient can be obtained from the integral of force autocorrelation function of a fixed molecule at an absolute position. However, the integrated values evaluated so in a finite system diminishes due to momentum flows arising from momentum conservation, and the diffusion coefficient diverges unphysically. We rigorously demonstrate that frequent removals of total momentum eliminate this flaw.